Simultaneous measurements of transport and poroelastic properties of rocks

Azar K. Hasanov, Manika Prasad, and Michael L. Batzle

Citation: Review of Scientific Instruments **88**, 124503 (2017);
View online: https://doi.org/10.1063/1.5018232
View Table of Contents: http://aip.scitation.org/toc/rsi/88/12
Published by the American Institute of Physics

Simultaneous measurements of transport and poroelastic properties of rocks

Azar K. Hasanov,[1,a)] Manika Prasad,[2] and Michael L. Batzle[1,b)]
[1]*Department of Geophysics, Colorado School of Mines, Golden, Colorado 80401, USA*
[2]*Department of Petroleum Engineering, Colorado School of Mines, Golden, Colorado 80401, USA*

(Received 28 November 2016; accepted 4 December 2017; published online 29 December 2017)

A novel laboratory apparatus has been developed for simultaneous measurements of transport and poroelastic rock properties. These transport and poroelastic properties at reservoir pressure and temperature conditions are required inputs for various geoscience applications, such as reservoir simulation, basin modeling, or modeling of pore pressure generation. Traditionally, the transport and poroelastic properties are measured separately using, for example, the oscillating pore pressure method to measure hydraulic transport properties, static strain measurements for elastic properties, and pore volumometry for storage capacity. In addition to time, the separate set of measurements require either aliquot cores or subjecting the same core to multiple pressure tests. We modified the oscillating pore pressure method to build an experimental setup, capable of measuring permeability, storage capacity, and pseudo-bulk modulus of rocks simultaneously. We present here the test method, calibration measurements (capillary tube), and sample measurements (sandstone) of permeability and storage capacity at reservoir conditions. We establish that hydraulically measured storage capacities were overestimated by an order of magnitude when compared to elastically derived ones. Our concurrent measurement of elastic properties during the hydraulic experiment provides an independent constraint on storage capacity. *Published by AIP Publishing.* https://doi.org/10.1063/1.5018232

I. INTRODUCTION

Hydraulic transport properties, permeability and storage capacity, control the passage and the storage of fluids in porous rocks. The evaluation of these primary properties is critical for reservoir characterization and simulation. An accurate reservoir simulation is essential for production forecast and economic analyses. Since the permeability and storage capacity are the main inputs into any reservoir simulations, they directly control the profitability of the petroleum reservoir, and their rigorous estimation is vital.

Elastic response of porous solids depends on a combination of confining and pore pressures, the so-called effective pressure. Since the pore pressure is not negligible in porous media, poroelastic properties depend also on the drainage condition. In this paper, we mostly deal with the drained poroelastic regime where the fluid is allowed to flow freely within and out of the pores. The drained bulk modulus, often considered equivalent to the bulk modulus of the room-dry porous rock frame is an important input in many rock physics workflows, including Gassmann fluid substitution. Drained poroelastic moduli also control phenomena, such as reservoir compaction and land subsidence, which can occur during hydrocarbon or water production (Geertsma, 1973). The storage capacity of reservoir rocks, defined as an undrained poroelastic modulus by some researchers (Green and Wang, 1990), also depends on effective pressure. Neglecting the pressure dependence of storage capacity during reservoir simulations may introduce errors in pore pressure and saturation predictions.

The oscillating pore pressure method has frequently been used to simultaneously measure the permeability and storage capacity of rocks (Kranz *et al.*, 1990; Fischer, 1992; Bernabé *et al.*, 2006; and Song and Renner, 2007). Relatively simple data reduction and continuous nature of the measurement are amongst the main advantages of this method. The method is based on measuring the amplitude ratio and the phase between the upstream and downstream pore pressure oscillations. Once these two parameters are obtained, it is possible to infer permeability and storage capacity from an analytical solution of the diffusivity equation with oscillatory boundary conditions (Kranz *et al.*, 1990; Fischer, 1992; Bernabé *et al.*, 2004; Bennion and Goss, 1971; and Faulkner and Rutter, 2000). A major drawback of this method is the uncertainty, sometimes exceeding an order in magnitude, in storage capacity estimation particularly when using a large downstream reservoir (Bernabé *et al.*, 2006).

The main objectives of this work are as follows:

- Study the feasibility of simultaneously measuring hydraulic and poroelastic properties by the pore pressure oscillation method.
- Describe the apparatus and experimental procedure.
- Perform a consistency check between hydraulically and elastically measured values of storage capacities.
- Provide proof of concept, test reliability, and errors, and benchmark our experiment using a capillary tube measurement.
- Report a sample dataset for sandstone as a function of oscillation frequency and effective stress to support our capillary tube observations.

a)Electronic mail: ahasanov@mines.edu
b)Deceased on 9 January 2015.

II. THEORETICAL BACKGROUND

A. Hydraulic transport properties

Darcy's law in its general form is the most commonly used relation to determine the steady-state flow permeability (Guéguen and Palciauskas, 1994),

$$\vec{q} = -\frac{\boldsymbol{k}}{\mu}\left(\nabla P_p + \rho_f \vec{g}\right), \tag{1}$$

where $\vec{q}$ is the Darcy velocity across the sample's cross-sectional area A, $\boldsymbol{k}$ is the permeability tensor of the porous medium, μ is the dynamic viscosity of the pore fluid, ∇P_p is the pore pressure gradient across the sample, ρ_f is the density of the fluid, and $\vec{g}$ is the acceleration due to the gravity. It follows from Eq. (1) that permeability defines the ability of porous media to transmit fluids when a pore pressure gradient is applied. By neglecting gravity effects and by assuming isotropic conditions, we evaluate the permeability tensor as a scalar property in this paper.

Part of the flowing fluid does not participate in the flow and is stored due to the contributions from fluid and pore space compressibilities. This phenomenon is described by the storage capacity coefficient. The storage capacity β_{st} is defined as the amount of fluid a porous medium stores or discharges due to a change in pore pressure under constant confining pressure (Wang, 2000 and Kümpel, 1991),

$$\beta_{st} = -\frac{1}{V_b}\left(\frac{\partial V_{fl}}{\partial P_p}\right)_{\delta P_c = 0}. \tag{2}$$

Here V_b is the volume of the rock, V_{fl} is the volume of the fluid, and $\delta P_c = 0$ denotes the constant confining pressure.

The most common way to measure the permeability of rocks is to apply constant flow rates and measure the pore pressure difference between upstream and downstream reservoirs (Kranz *et al.*, 1990). The permeability is then computed using Darcy's law. This method however may not be suitable for tight rocks since a long period of time is needed to achieve a steady state flow regime. To overcome this obstacle, Brace *et al.* (1968) introduced the pressure pulse-decay or transient step method. In a typical experiment, a sample is placed between upstream and downstream reservoirs and subjected to a time-dependent increase in the upstream pressure. Depending on the permeability and storage capacity of the sample, the propagating pressure front achieves a steady-state condition after a transient period. The solution of the transient part of the diffusion equation yields simultaneous estimation of both permeability and storage capacity (Hsieh *et al.*, 1981).

The pulse-decay method has several drawbacks. First, the method requires long periods of pressure re-equilibration between measurements. Second, interpretation of results can be easily distorted by noisy readings (Fischer, 1992), especially in low-permeability samples. Possible sources of noise include temperature variations (these experiments should be performed at isothermal conditions) or leaks in the apparatus. Since the upstream and the downstream pressures are essentially either a step function or a linear increase, the Fourier-transformed frequency spectrum of these signals contains all frequencies. Thus, the pulse-decay method is insensitive to any specific frequency, and noise filtering for signal enhancement in the frequency domain is not possible. Replacing the step function with a time-harmonic upstream pressure at a specific frequency can eliminate many noise issues.

The main difference between the pore pressure oscillation method and the pulse-decay method lies in the boundary conditions to solve the diffusion equation. In the experimental procedure, a jacketed sample is placed in a pressure vessel and connected to the upstream and downstream reservoirs. It is saturated at elevated pore pressures to ensure full saturation. Finally, time-harmonic pressure excitation is applied to the sample. The time-harmonic excitation allows digital signal enhancement through frequency filtering. The excitation is achieved by inducing an upstream pressure oscillation upon the background pore pressure by servo-controlled intensifiers (Song and Renner, 2007) or in our case, directly by a frequency modulated on a pore pressure pump. During propagation through the porous medium, the pore pressure oscillation undergoes attenuation. Consequently, the pressure disturbance detected at the downstream face exhibits a phase shift and a reduced amplitude. The phase shift θ and downstream-to-upstream pressure amplitude ratio R, obtained via Fourier analysis, are needed to solve for the permeability and storage capacity of the sample.

Kranz *et al.* (1990) and Fischer (1992) have derived an analytical solution for the diffusion equation with oscillatory boundary conditions. Here, we follow their analytical solution with the amplitude ratio and phase expressed in terms of dimensionless permeability η and dimensionless storage capacity ξ (Bernabé *et al.*, 2006),

$$\eta = \frac{2A}{\omega L \mu \beta_d} k, \quad \xi = \frac{AL}{\beta_d}\beta_{st}, \tag{3}$$

where A is the sample cross-sectional area, L is the length, ω is the angular frequency of oscillation, μ is the dynamic viscosity of the pore fluid, and β_d is the storage capacity of the downstream reservoir. The solution for the amplitude ratio and phase is (Bernabé *et al.*, 2006)

$$R = \left|\left(\cosh\left[\sqrt{\frac{\xi}{\eta}}(1+i)\right] + \frac{(1+i)}{\sqrt{\xi\eta}}\sinh\left[\sqrt{\frac{\xi}{\eta}}(1+i)\right]\right)^{-1}\right|,$$
$$\theta = \arg\left[\left(\cosh\left[\sqrt{\frac{\xi}{\eta}}(1+i)\right] + \frac{(1+i)}{\sqrt{\xi\eta}}\sinh\left[\sqrt{\frac{\xi}{\eta}}(1+i)\right]\right)^{-1}\right]. \tag{4}$$

The amplitude ratio and phase are measured experimentally; η and ξ are derived by solving the system of Eq. (4) numerically using an iterative error-minimizing approach; and permeability and storage capacity are calculated using Eq. (3).

The (η, ξ) solution space in the (R, θ) domain (Fig. 1) reveals the advantage of using these dimensionless parameters. Given the relationships in Eq. (3), the iso-ξ and iso-η lines can be taken to also represent storage capacity and permeability isolines. The solution space is bounded by $\xi = 0$ and $\xi = +\infty$ lines. The size of the downstream reservoir plays a vital role in detecting pressure amplitudes and phases. A large downstream reservoir storage shifts the possible solution toward the $\xi = 0$ isoline, thus rendering the experiment much less

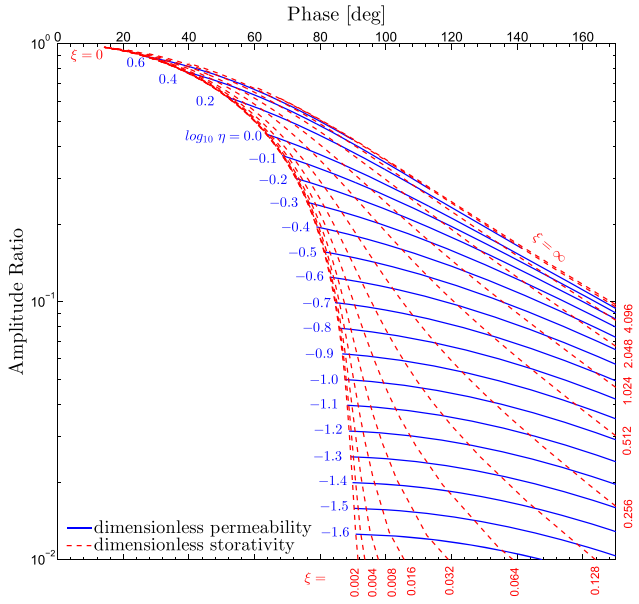

FIG. 1. The plot of iso-ξ (dashed red) and iso-η (solid blue) lines as functions of amplitude ratio and phase shift represents the possible solutions of Eq. (4). Reprinted with permission from Bernabé *et al.* (2006), Int. J. Rock Mech. Min. Sci. **43**, 311–316 (2006). Copyright 2006 Elsevier Ltd.

sensitive to the sample's storage capacity. Since high permeability rock samples require a large downstream reservoir in order to record sufficient amplitude ratios and phases (ideally we want to avoid the narrow solution "tail"), the resolution in their storage capacity measurement is sacrificed. On the other hand, the successful measurement of low-permeability tight rocks necessitates small downstream reservoirs. In any case, determination of permeability does not suffer from the downstream reservoir size since iso-η lines run almost perpendicular to the $\xi = 0$ isoline.

B. Poroelastic properties

Permeability measurements can be benchmarked against values derived from the constant flow method. However, benchmarking the storage capacity measurements can be challenging, given the paucity of comparable data. We used poroelastic theory to derive comparable data. The upstream pore pressure oscillation applied in our work also causes bulk deformation of the sample. The poroelastic modulus K_{bp} [also called Biot poroelastic expansion coefficient H (Kümpel, 1991)] characterizes the bulk volumetric deformation caused by an increase in pore pressure at constant confining pressure and has been defined by [Zimmerman *et al.* (1986)]

$$\beta_{bp} = \frac{1}{K_{bp}} = -\frac{1}{V_b}\left(\frac{\partial V_b}{\partial P_p}\right)_{\delta P_c = 0}. \tag{5}$$

Once K_{bp}, sometimes called pseudo-bulk modulus (Zimmerman *et al.*, 1986), is known, then all the drained and undrained poroelastic moduli, including the storage capacity can be calculated, with prior information about porosity ϕ, unjacketed K_s, and fluid K_{fl} bulk moduli. The relations for the poroelastic moduli, drained frame bulk modulus K_{bc}, Biot's coefficient α, Skempton's coefficient B, and storage capacity β_{st} (Zimmerman *et al.*, 1986 and Kümpel, 1991) are

$$\beta_{bc} = \frac{1}{K_{bc}} = \frac{1}{K_{bp}} + \frac{1}{K_s}, \tag{6}$$

$$\alpha = \frac{K_{\min}}{K_{bp} + K_s}, \tag{7}$$

$$B = \frac{1}{1 + \phi\left(\frac{K_{bp}}{K_{fl}} - \frac{K_{bp}}{K_s}\right)}, \tag{8}$$

$$\beta_{st} = \frac{1}{K_{bp}} + \phi\left(\frac{1}{K_{fl}} - \frac{1}{K_s}\right), \tag{9}$$

where the fluid compressibility (inverse of fluid bulk modulus) is defined as $1/K_{fl} = -1/V_{fl}\left(\partial V_{fl}/\partial P\right)$ and solid compliance (inverse of the unjacketed bulk modulus) is $1/K_s = -1/V_b\left(\partial V_b/\partial P_p\right)_{\delta P_c - \delta P_p = 0}$. Although poroelastic moduli are commonly defined in terms of unjacketed bulk modulus, this rock property is poorly understood and rarely measured (Wang, 2000 and Mavko *et al.*, 2009). Instead, we assume for simplicity that the unjacketed bulk modulus equals to mineral bulk modulus, defined as $1/K_{\min} = -1/V_{\min}\left(\partial V_{\min}/\partial P\right)$ and computed from using the Voigt-Reuss-Hill averaging scheme using measured mineralogy. Theoretically, the assumption $K_s \equiv K_{\min}$ should be valid for monomineralic rocks. However, experiments have shown that the presence of clays may cause the measured unjacketed bulk modulus to differ significantly from Voigt-Reuss-Hill computed values (Hofmann and Batzle, 2005 and Makhnenko and Labuz, 2013). Even nanocrystalline intergranular material of the same mineral composition may exhibit different elastic behavior (Wagner *et al.*, 2011). In this paper, we present an example dataset for a clean sandstone sample to minimize the uncertainty in the mineral bulk modulus.

Measurements of the poroelastic deformation in response to the pore pressure oscillation provide an independent consistency check of hydraulically measured storage capacity values. Biot and Skempton coefficients can be expressed in terms of storage capacity, providing an indirect benchmarking of storage capacities,

$$\alpha = 1 - \frac{1}{K_{\min}}\left(\frac{1}{\beta_{st} + \frac{(1+\phi)}{K_{\min}} - \frac{\phi}{K_{fl}}}\right), \tag{10}$$

$$B = 1 - \frac{\phi}{\beta_{st}}\left(\frac{1}{K_{fl}} - \frac{1}{K_{\min}}\right). \tag{11}$$

Biot and Skempton coefficients are always constrained between 0 and 1; high values of both parameters intuitively indicate a soft, unconsolidated rock, whilst stiff low-porosity rocks usually yield low α and B values.

We record the pore pressure oscillation-induced volumetric deformation with axial and radial strain gauges (see Fig. 2). We compute volumetric strains ε_v using the following relationship:

$$\varepsilon_v = \varepsilon_a + 2\varepsilon_r, \tag{12}$$

where ε_a is the axial strain and ε_r is the radial strain. The poroelastic modulus measured directly in such an experiment is Zimmerman's pseudo-bulk modulus K_{bp}. Note that K_{bp} is

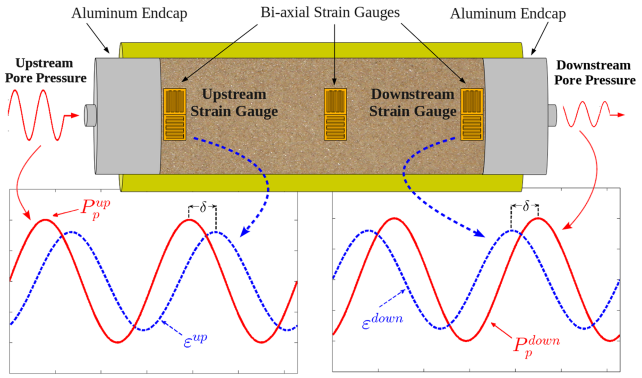

FIG. 2. An illustration of the strain response, recorded by the upstream and downstream pairs of strain gauges and generated by propagating through the sample pore pressure oscillation.

complex necessitated by causality with the time-harmonic pore pressure,

$$K_{bp}^*(\omega) = \frac{P_p^0(\omega)}{\varepsilon_v^0(\omega)} e^{i(\omega t+\theta)}, \tag{13}$$

where $\varepsilon_v^0(\omega)$ is the frequency-dependent volumetric strain response to the oscillatory pore pressure.

III. EXPERIMENTAL APPROACH

A. Sample preparation

The samples were cut into cylinders of approximately 25 mm diameter and 100-140 mm length. Due to their high gas permeability, we increased sample lengths to maximize amplitude ratios and phase lags. Every sample was instrumented with strain gauges (bi-axial OMEGA foil strain gauges) for simultaneous measurements of poroelastic moduli. To attach strain gauges, the surface of the sample (except the upstream and the downstream sides) was coated with K-20 epoxy and a Kapton polyimide film. This precaution prevented the outflow of the pore fluid and subsequent damage to the strain gauges. The bi-axial foil strain gauges consist of two orthogonal resistor networks, and hence such gauges allow us to measure longitudinal and transverse deformations simultaneously. Three pairs of strain gauges were glued onto the Kapton-covered surface of the sample: one each closest to the upstream and the downstream sides and the third strain gauge in the middle of the sample (see Fig. 2). The samples were also instrumented with thermocouples for real-time temperature monitoring of the experiment (not shown in the sample schematics).

After strain gauges were attached, the sample was clamped between two aluminum endcaps with groves on the faces adjacent to the sample for even fluid distribution and diffusion into the sample. The entire sample-aluminum assembly was then cast with flexible epoxy resin to form an impermeable jacket. This impermeable epoxy jacket prevented the confining pressure fluids entering and the pore pressure fluid escaping the sample.

B. Experimental setup

The experimental apparatus, depicted in Fig. 3, consists of a pressure vessel (rated to working pressure up to 69 MPa), two pressure pumps, a function generator, three pressure transducers, strain gauge preconditioning modules, differential amplifiers, a digitizing unit, and a personal computer. In a typical experiment, a jacketed sample is mounted on the pressure vessel head and placed inside the pressure vessel filled with hydraulic oil. The sample is then vacuumed for at least 2 h. Once the sample is evacuated, we increase the confining

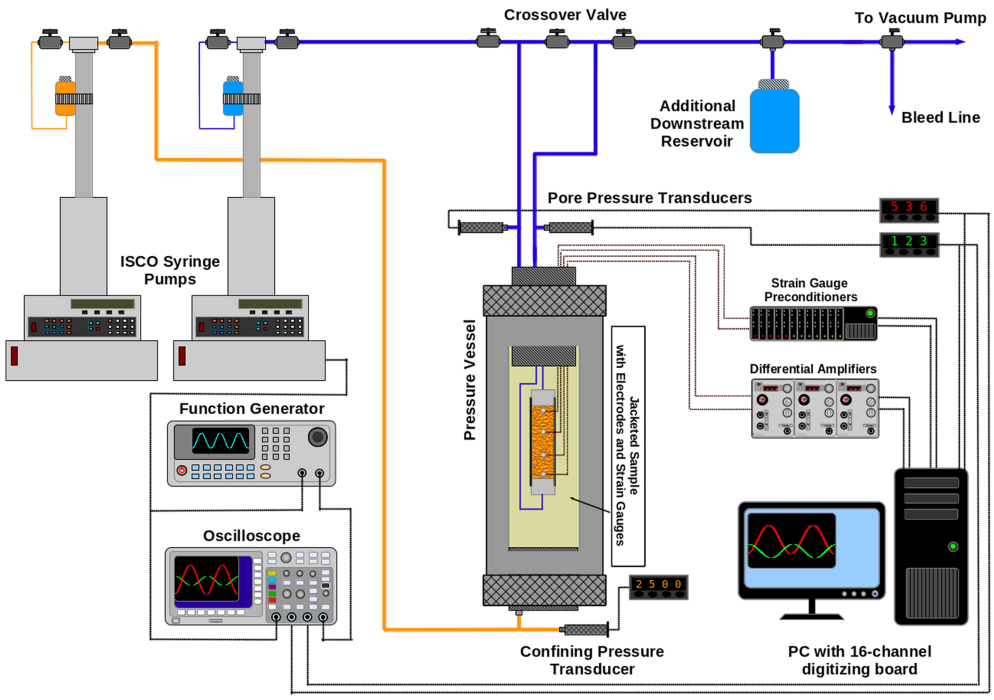

FIG. 3. Experimental setup used for measurements at reservoir conditions.

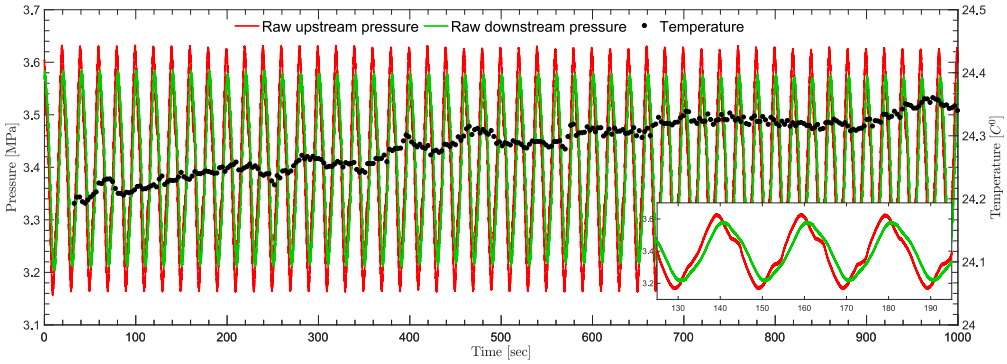

FIG. 4. A chart of raw upstream and downstream pore pressures, overlaid with the temperature record. The temperature data have been smoothed over 20 s time-interval and indicate temperature variation of less than 0.2 °C during the course of the experiment. The data are shown for the Navajo 7 sample at 62 MPa differential pressure and 50 mHz oscillation frequency.

pressure to 5 MPa at a rate of 0.3 MPa/min and saturate it with deionized water at elevated pore pressure (3.45 MPa). The elevated pore pressure and a soak time of an hour ensure saturation and dissolution of any air bubbles. After saturating the sample, we modulate an oscillation on the constant pore pressure of 3.45 MPa. The amplitude of the pore pressure oscillation is maintained below ten percent of the background pore pressure (0.35 MPa in our case) to avoid irreversible inelastic changes in a rock (Kranz *et al.*, 1990).

We first benchmarked the setup with a capillary tube experiment at "benchtop" conditions, that is, at ambient temperature and atmospheric pressure conditions. The capillary tube was encased in a flexible epoxy mold to prevent fluid pressure leaks and connected to pore pressure fluid lines on the table top. Fluid pressure oscillations were excited at 0.2 MPa; oscillation amplitudes did not exceed 0.1 MPa.

Two OMEGA PX612 pressure transducers, recording upstream and downstream pore pressures, are connected to the pressure vessel head through pore pressure plumbing. A third pressure transducer is placed at the bottom of the pressure vessel and records the confining pressure. After preconditioning and amplification by OMEGA DB25 strain meter units, the electrical output signals from upstream and downstream pressure transducers are recorded and digitized by an MC USB-1608G data acquisition card. The upstream pore pressure plumbing is connected to a Teledyne ISCO 100DX syringe hydraulic pressure pump; the downstream side is connected to the downstream reservoir. An Agilent 33250A function generator is used to modulate an analog voltage on the pump to generate pore pressure oscillations. The amplitude, frequency, and DC offset of the oscillations are controlled with the function generator. Electrical voltage signals, generated by strain gauges when the sample deforms, are filtered, amplified by the Validyne SG297A strain gauge preconditioning module, and digitized by the data acquisition card. The size of the downstream reservoir can be adjusted using the three 250 cm^3 aluminum reservoirs installed in series. The downstream reservoir with an adjustable volume increases the permeability range measurable by our apparatus.

The experiment should ideally be conducted under isothermal conditions since temperature fluctuations can cause a significant change in pore pressure and lead to inaccurate measurements. Temperature control is particularly important for low-permeability rocks that require longer experiment times. To avoid temperature fluctuations, the pressure vessel, the downstream reservoirs, and the pore pressure plumbing lines were thermally insulated with a fiberglass pipe insulation material. Figure 4 presents the sample records of oscillating pore pressure and temperature. During the experiments, temperature variations remained below 0.5 °C. The pressure perturbations caused by these temperature variations are negligible and filtered out by frequency-domain filtering.

C. Data processing

Our experimental setup measures pore pressures, volumetric strains, and temperatures simultaneously. Since we record pressures and strains as time series of voltage (e.g., generated by deforming strain gauges), the data processing procedure described below was common to all the measurements, except for the temperature data. Instead, the standard moving-average smoothing has been applied to the acquired temperature data (see Fig. 4).

The data processing workflow starts with noise removal by filtering the recorded voltage signals. The apparatus is driven by pore pressure sinusoids and has a roughly linear response below the critical Biot frequency. Although the pore pressure and strain responses should also be sinusoidal, noise-contamination makes the recorded time-series quasi-sinusoidal. Tardif *et al.* (2011) mentioned that small deflections from the purely sinusoidal signal may be produced by either piston friction or non-linear effects of the apparatus. The non-linear effects become increasingly pronounced at higher frequencies (higher than 300 mHz in our setup), resulting in greater departure from sinusoidal behavior of the recorded data.

The data acquisition is usually run for 30-35 cycles in order to reach the steady-state regime of fluid flow through the sample (Bernabé *et al.*, 2006). The transient part of the data is generally excluded from the analysis of permeability and storage capacity. Amplitude ratios and phases calculated at each sampling time by moving-window FFT (Fast Fourier Transform) analysis and plotted as functions of time [see Fig. 5(b)] reveal the steady-state nature of the late-time pressure response and verify that the early-time transient signal has been eliminated.

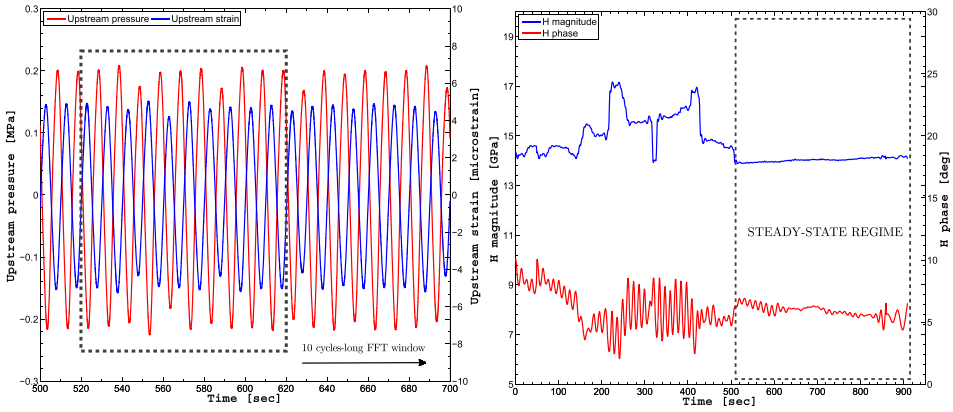

(a) (b)

FIG. 5. Moving-window FFT analysis of sample strain data; 100 mHz oscillation frequency at 62 MPa differential stress. (a) Filtered upstream pressure and upstream strain time-series. The FFT analysis is performed by a ten cycle-long moving window. (b) The magnitude and phase of the poroelastic expansion coefficient H as functions of time, calculated by the moving-window FFT analysis. The mean and standard deviations are calculated from the late-time, steady-state response.

We use a bandpass frequency filter in the Fourier domain to eliminate noise. We first convert the recorded data from time domain into frequency domain using Fast Fourier Transform (FFT) and then apply a digital bandpass Butterworth filter to the late-time pressures. Due to the time-harmonic nature of pore pressure oscillations, the frequency domain filter eliminates most of the noise in the data. The filtered signal is converted back into time series by Inverse Fast Fourier Transform (IFFT) and used to calculate hydraulic and poroelastic properties.

We determine the amplitude ratio (R) by dividing the downstream pore pressure amplitude by the upstream pressure amplitude at the dominant oscillating frequency; the phase shift between downstream and upstream signals (θ) is determined by the cross-power spectral density method. Once we obtain the values of the amplitude ratio and phase shift, we solve Eq. (4) for dimensionless parameters and subsequently calculate the permeability and storage capacity of the sample using Eq. (3).

The strain data are processed similar to the pore pressure data, namely, bandpass filtering to eliminate noise. They are converted into strain values using the following formulas:

$$\varepsilon_{cal} = \left[\frac{1}{GF}\right]\left[\frac{R_g}{R_{cal}+R_g}\right], \tag{14}$$

$$\varepsilon_{rock} = \left[\frac{\varepsilon_{cal}}{\Delta V_{cal}}\right]\Delta V, \tag{15}$$

where ε_{cal} is the calibrated microstrain, GF is the gauge factor, R_{cal} is the shunt resistance, R_g is the strain gauge resistance, ε_{rock} is the actual rock strain, ΔV_{cal} is the voltage change measured during calibration with a shunt resistor (4.3 V), and ΔV is the voltage change generated during the experiment. The poroelastic expansion coefficient K_{bp} is then computed using Eq. (13), i.e., dividing the amplitude of pore pressure by the amplitude of strain (either upstream or downstream) at the dominant frequency.

D. Uncertainty quantification

We estimated absolute errors in hydraulic transport and poroelastic properties by calculating the standard deviation in the acquired data consisting of pressure and strain time-series. We also estimated uncertainty by considering oscillation frequencies. We calculated frequency-dependent errors by analyzing data gathered at various frequencies. The procedure involves calculating amplitude ratios (R), phases (θ), and poroelastic expansion coefficients (H) at every time step of the recorded waveforms by moving-window FFT analysis. The five to ten cycle-long time-window is centered around a certain time step. A step-by-step procedure to calculate absolute errors in the poroelastic expansion coefficient is as follows:

1. Window the recorded strain and pore pressure time series.
2. Filter out the noise with a bandpass filter.
3. Perform Fourier transformation of the time-window.
4. Evaluate Eq. (13): In this case, divide the pressure amplitude at the corresponding peak frequency by the volumetric strain.
5. Obtain the poroelastic expansion coefficient K_{bp} as a function of time.
6. Calculate the mean and the standard deviation of the steady-state part. The ratio of the standard deviation to the mean is the absolute error of the measurement.
7. Perform time-windowed cross-power spectral density analysis (cross-FFT) if the parameter of interest is a phase angle (e.g., phase lag between upstream and downstream pressures, upstream strain, and upstream pressure). The size of the moving-window and example results are demonstrated in Fig. 5. The moving-window FFT analysis has been performed for every recorded frequency to obtain frequency-dependent errors and possibly a regression equation between the oscillation frequency and the absolute error.

Figure 6 summarizes the calculated frequency-dependent errors in the pore pressure amplitude ratio and in magnitudes and phase angles of the poroelastic expansion coefficient. The analysis has been performed on Fox Hills 7 data at three differential stresses (3.5, 34.5, and 62 MPa). The errors for all samples were identical; hence we present only the results for the Fox Hills 7 sample. The uncertainty in both amplitude ratios and phase lags for pore pressures increases with oscillation frequencies and follows a cubic law. The errors in phase measurement are much larger than those in amplitude ratio, reaching almost 25% at highest frequencies. The error in the magnitude of the poroelastic expansion coefficient

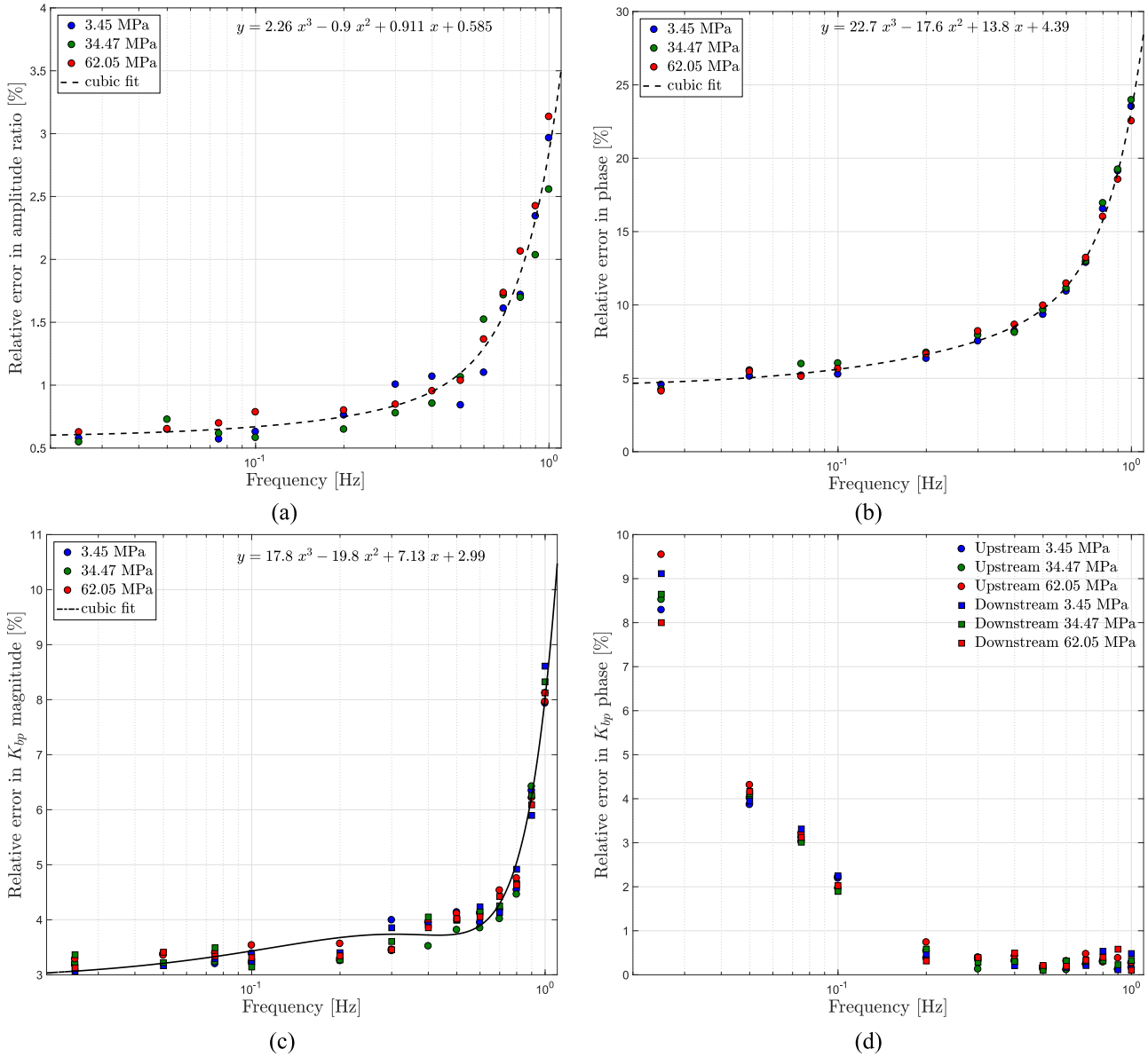

FIG. 6. Frequency-dependent relative errors in the amplitude ratio and phase lag of pore pressure data, as well as in the magnitude and phase of the poroelastic expansion coefficient using data for the Fox Hills 7 sample at various differential pressure steps as functions of oscillation frequencies. (a) Error in amplitude ratios of measured pore pressures. (b) Error in phase shifts of measured pore pressures. (c) Error in the magnitude of measured poroelastic expansion coefficient. (d) Error in the phase of measured poroelastic expansion coefficient.

increases and the phase angle decreases with increasing oscillation frequency [see Figs. 6(c) and 6(d)].

We further propagate the errors in the poroelastic expansion coefficient to calculation of other poroelastic properties, assuming a conservative absolute error of 5% in mineral frame and fluid bulk moduli and 10% in porosity. These uncertainties are calculated as standard deviation (σ_x) using the standard error propagation equation (Philip and Robinson, 2003),

$$\sigma_x = \sqrt{\sigma_u^2 \left(\frac{\partial x}{\partial u}\right)^2 + \sigma_v^2 \left(\frac{\partial x}{\partial v}\right)^2 + \cdots}, \tag{16}$$

where x is the function of variables u and v, and σ_u and σ_v are the standard deviations associated with u and v, respectively.

Permeability and storage capacity calculations involve solving a highly non-linear set of equations (4). Thus, the uncertainty estimation of these parameters becomes non-trivial and cannot be performed using Eq. (16). We assess uncertainties in permeability and specific storage using the method described in the work of Bernabé *et al.* (2006). Here we briefly outline the main steps of this approach:

1. Based on the standard deviation estimations for pressure amplitude ratio (δR) and for phase angles ($\delta\theta$), we create Gaussian data realizations $\{R_i + \mathcal{G}(\frac{\delta R}{2})\}$ for amplitude ratios and $\{\theta_i + \mathcal{G}(\frac{\delta\theta}{2})\}$ for phase lags. Here R_i and θ_i are the values from the experiment; $\mathcal{G}(\sigma)$ is a zero-mean Gaussian noise with a standard deviation σ. We perform this step for each oscillation frequency step since as mentioned before, the relative errors in amplitude ratio and phase increase non-linearly with frequency. We use cubic-fit equations from Fig. 6 to approximate

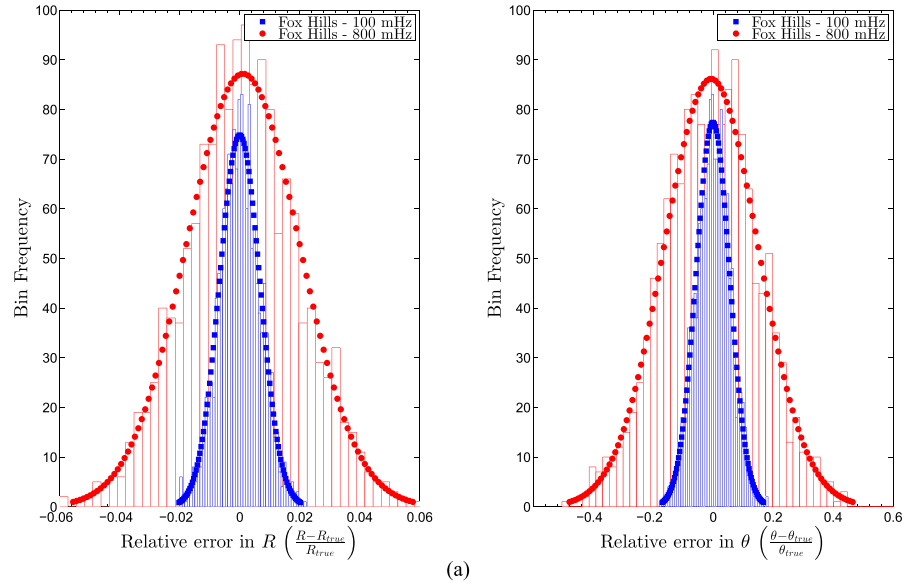

(a)

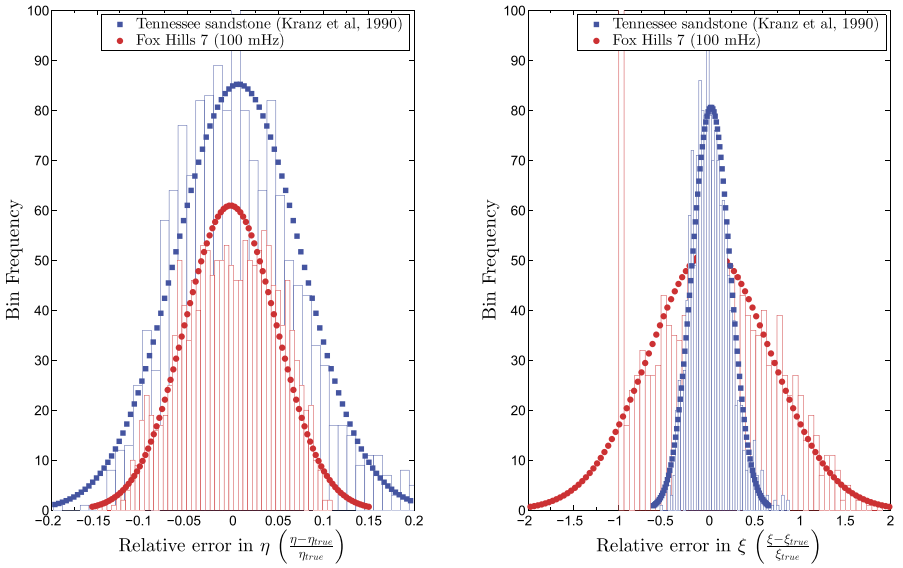

(b)

FIG. 7. Simulated errors in hydraulic properties using the Gaussian distribution of errors in the amplitude ratio and phase. (a) Gaussian data realizations of amplitude ratios and phase angles at 100 and 800 mHz oscillation frequencies. Note much broader distribution of data at 800 mHz frequency. The realizations are shown for the Fox Hills 7 sample at 3.45 MPa differential stress. (b) Statistical distribution of the relative error in η and ξ; comparison between the literature data [Tennessee sandstone from Kranz *et al.* (1990)] and Fox Hills 7 sandstone; 100 mHz oscillation frequency at 3.45 MPa differential pressure.

frequency-dependent relative errors in amplitude ratio and phase lag. Figure 7(a) demonstrates this frequency-dependence: the distribution of normalized amplitude ratio and phase shift is much broader at higher oscillation frequencies.

2. We solve the system of Eq. (4) for every (R, θ) realization pair and recover the Gaussian distribution of dimensionless permeability η and dimensionless storage capacity ξ. The standard deviation of a normal distribution curve fitted to the $(\frac{\eta-\eta_{true}}{\eta_{true}}, \frac{\xi-\xi_{true}}{\xi_{true}})$ Gaussians gives us the relative error of each dimensionless number.
3. Once the relative errors in η and ξ are known, we propagate the uncertainties into permeability and storage capacity [Eq. (16)]. Note that since the relative errors in all other parameters (length and cross-sectional area of samples, fluid viscosity, oscillation frequency, and downstream reservoir storage capacity) are negligible, we can assume the errors in permeability and specific storage to be equal to the errors in η and ξ.

Following this methodology, we estimate the relative errors in η and ξ for all samples measured in this research. The uncertainties were calculated for the whole frequency sweep at three differential stress steps (3.45, 34.47, and 62.05 MPa). For comparison, we also calculated uncertainties in η and ξ for Tennessee sandstone data (Kranz *et al.*, 1990). We used the errors in amplitude ratio $\delta R = 2 \times 10^{-3}$ and phase shift $\delta\theta = 10.8°$ and measured values of $R_i = 0.07$ and $\theta_i = 135°$, as mentioned in the paper. Figure 7(b) compares the errors in the Tennessee and Fox Hills 7 data sets at 100 mHz. While the errors in η are similar, the errors in ξ for Fox Hills 7 are almost four times greater than those for Tennessee sandstone. This discrepancy might be a consequence of large downstream storage capacity of our apparatus. In Sec. II A, we demonstrate that a large downstream reservoir shifts the possible solution for ξ toward the $\xi = 0$ bound of the solution space (see Fig. 1), reduces the resolution of storage capacity estimation, and increases uncertainty while η estimates are relatively insensitive. Hence, a large downstream reservoir causes the

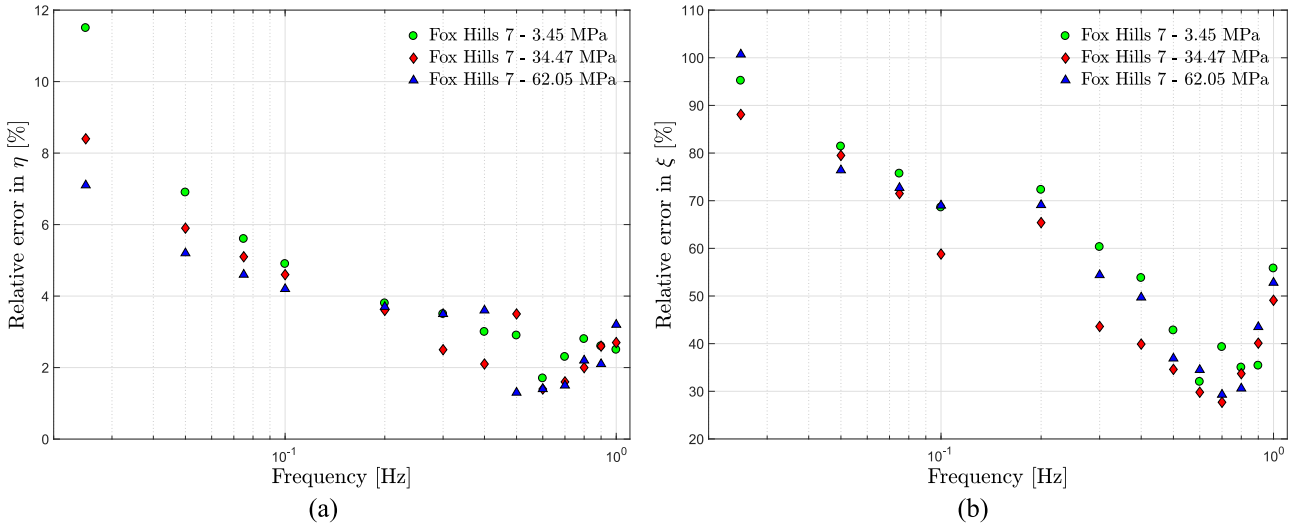

FIG. 8. Frequency-dependent relative errors in dimensionless permeability and storage capacity. (a) Relative errors in dimensionless permeability, derived for three samples at three differential stress steps as a function of the oscillation frequencies. (b) Relative errors in dimensionless storage capacity, derived for three samples at three differential stress steps as a function of the oscillation frequencies.

large uncertainty in ξ and small error (≈5%) in η for Fox Hills 7. This analysis proves the accuracy of permeability measurements with the pore pressure oscillations. Further, it shows that the errors in ξ are generally much greater than those in η (see Fig. 8).

The estimated uncertainties in storage capacity are high, reaching almost 100% at the lowest oscillation frequency and often exceeding 50%. Thus, storage capacity estimates derived using the hydraulic pore pressure oscillation experiment are not trustworthy by themselves, particularly when compared to the relative errors of oscillating strain-derived storage capacity with errors below 7%. In contrast, the accuracy of permeability measurements is confirmed by the low relative errors, reaching a maximum of 12% at the lowest oscillation frequency. The errors in the frequency range of interest (100–300 mHz) are consistently less than 10%.

IV. RESULTS

A. The capillary tube experiment

As a proof of concept of the experimental setup and to test the reliability of our measurements, we conducted a benchtop oscillating pore pressure experiment on a single capillary of known dimensions. Both static and dynamic permeabilities of a capillary tube can be analytically calculated. Johnson *et al.* (1987) provided the formula of frequency-dependent permeability for a single capillary tube of radius r,

$$\tilde{k}(\omega) = k_0 \left[\frac{8}{(Kr)^2} \left(\frac{2}{Kr} \frac{J_1(Kr)}{J_0(Kr)} - 1 \right) \right], \tag{17}$$

where $k_0 = \phi r^2/8$ is the DC permeability, $K^2 = i\omega\rho_f/\mu$, r—radius of the capillary, and J_0 and J_1 are the Bessel functions of the order zero and one, respectively.

The storage capacity of a single capillary tube is given by (for derivation see the Appendix)

$$\beta_{st} = \frac{2}{3K_{\min}} \left(\frac{1+\nu_{\min}}{1-2\nu_{\min}} \right) + \frac{1}{K_{fl}}, \tag{18}$$

where $K_{\min}$ is the bulk modulus and $\nu_{\min}$ is Poisson's ratio of glass; K_{fl} is the bulk modulus of fluid. Assuming that K_{fl} = 2.38 GPa and properties of glass are $K_{\min}$ = 36 GPa and $\nu_{\min} = 0.16$, we calculated the storage capacity of the capillary tube to be equal to $\beta_{st} = 4.596 \times 10^{-10}$ Pa^{-1}. The length of the capillary was 103.5 mm; the diameter was 210 μm, as revealed by X-ray computed microtomography (μ-XCT) scan. The experiment has been conducted at nine oscillation frequencies: 0.05, 0.1, 0.15, 0.25, 0.3, 0.4, 0.5, 0.6, and 0.7 mHz.

Figure 9(a) shows the results of the permeability measurements. Equation (17) predicts a DC permeability of the capillary to be 1.37×10^{-9} m^2 which starts to decline at the critical Biot frequency of 117 Hz [the critical Biot frequency is $\omega_c = 8\mu/\rho_f r^2$, where r is the tube radius (Hughes *et al.*, 2003)]. The permeability values at the first three oscillation frequencies closely follow the predicted dynamic permeability curve; however, a strong increase of measured permeabilities is observed starting from 0.25 mHz frequency.

Figure 9(b) demonstrates that the measured storage capacity values are overestimated, diverging from the calculated storage capacity of the capillary tube [see Eq. (18)] by almost five orders of magnitude. Again, the strong discrepancy in measured storage capacity is due to the large downstream reservoir. Using a high storage capacity downstream reservoir significantly increased the error in the measured storage capacity. Storage capacity data based only on the oscillating pore pressure experiment are unreliable. Independent measurements are required to constrain the hydraulically measured storage capacities.

B. Frequency dependence

Johnson *et al.* (1987), Sheng and Zhou (1988), and Zhou and Sheng (1989) have shown that the dynamic permeability of

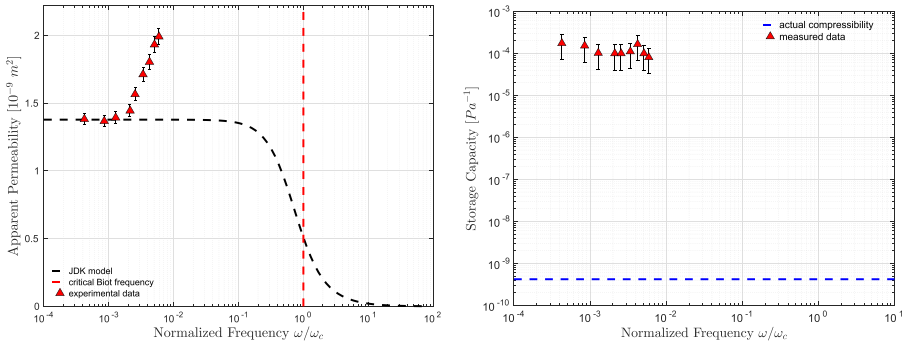

FIG. 9. (a) Permeability and (b) storage capacity of a single capillary with 210 μm diameter, measured at various oscillation frequencies. The oscillation frequencies are normalized by the critical Biot frequency ω_c of 117 Hz. The dynamic permeability curve is calculated from the JDK model (Johnson *et al.*, 1987). Obtained values of storage capacities are highly overestimated since the storage capacity for this capillary is $\beta_{st} = 4.6 \times 10^{-10}$ Pa^{-1} (see the Appendix).

porous media approaches the DC limit at oscillation frequencies below Biot's critical frequency. Our apparatus operates in the frequency range of 0.001–1 Hz, well below Biot's critical frequencies for typical sedimentary rocks [kiloHertz range as per Pride (2005)]. The storage capacity derived from the hydraulic aspect of the oscillatory pore pressure experiment should not be frequency-dependent. According to Eq. (3), the dimensionless storage capacity number ξ calculation does not involve the frequency of the oscillation. Thus, amplitude ratios and phases of the upstream and downstream pore pressure sinusoids at different frequencies should theoretically lie on a single iso-ξ line (see Fig. 1).

Despite the theoretical independence of permeability and storage capacity on the oscillation frequency in the range of our experiments, we observe a distinct relation of the measured parameters to the oscillation period. Permeabilities tend to fluctuate around a certain value at lower frequencies and steadily increase beyond oscillation frequencies of 0.3 Hz. The measured storage capacities seem to decrease with increasing frequencies, attain a local minimum, and then increase again. Although Subsection III D presents large relative errors in storage capacities and low overall reliability of the hydraulically derived storage capacity data, we do not attribute the apparent frequency-dependence of the measured hydraulic properties to the measurement uncertainty—the values of permeabilities do not fall within the error limits. Figures 10(a) and 10(b) summarize the measured data as a function of oscillation frequency at 3.45 MPa differential pressure step for the sandstone sample Fox Hills 7.

There appears to be a physical reason for the observed frequency dependence. Prior studies by Bernabé *et al.* (2004) and Song and Renner (2007) also show a dependence of measured permeabilities and storativities on the period of the input pore pressure oscillations. The reported frequency-dependence of the data (Bernabé *et al.*, 2004) resembles our findings [see Fig. 3 in Bernabé *et al.* (2004)]. The few papers on experimental observations of frequency-dependent permeability and storage capacity under oscillating pore pressures [e.g., Rigord and Caristan (1993) and Song and Renner (2006)] suggest that the apparent frequency-dependence is caused by heterogeneities. Our results on the capillary tube experiment dispel this argument; we postulate the observed effect to be either caused by partial saturation of the capillary (an air bubble) or an internal resonance of the pressure pump. Note that since the rock measurements are made at high pore pressures, partial saturation might not play a role. Kurzeja *et al.* (2016) suggested that tube deformation might explain the deviation of capillary tube permeability from the steady-state value at frequencies above the critical frequency. In future work, we will repeat the capillary measurements at high pore pressures, perhaps followed by a finite-element fluid flow simulation in a heterogeneous permeability field.

C. Pressure dependence

Microcracks influence transport and elastic properties of rocks significantly (Walsh, 1965; Batzle *et al.*, 1980; and Guéguen *et al.*, 2011). In typical sedimentary reservoir rocks, such as sandstone, porosity is conceptualized as a combination of equant (spherical) pores and elliptical cracks with various aspect ratios. These microcracks also cause permeability, storage capacity, and poroelastic moduli to be dependent on effective stress. The commonly observed sharp change in transport and elastic properties of sedimentary rocks at early stages of loading is attributed to the closure of microcracks (Batzle *et al.*, 1980).

1. Permeability

Permeability decreases with increasing differential pressure during hydrostatic loading due to the closure of microcracks and thus creating a more tortuous flowpath and increasing the resistance to flow. Figure 10(c) summarizes our permeability results for the Fox Hills 7 sample measured at 0.1 Hz pore pressure oscillation frequency as a function of loading and unloading differential hydrostatic pressures.

2. Hydraulically derived storage capacity

These results are ambiguous and inconclusive due to the high experimental error when using a large downstream reservoir. The microcrack closure is also responsible for decreasing the storage capacity with increasing effective stress—the rock is basically able to store less fluids, and this effect can be observed in Fig. 10(d), although this decrease is not very clear.

3. Stiffness

Stiffness increases significantly with effective stress due to the closure of compliant pores and cracks. This increase is more pronounced at lower pressures and manifests itself as a sharp increase in elastic moduli. Once the compliant microcracks are closed, the pressure-dependence becomes

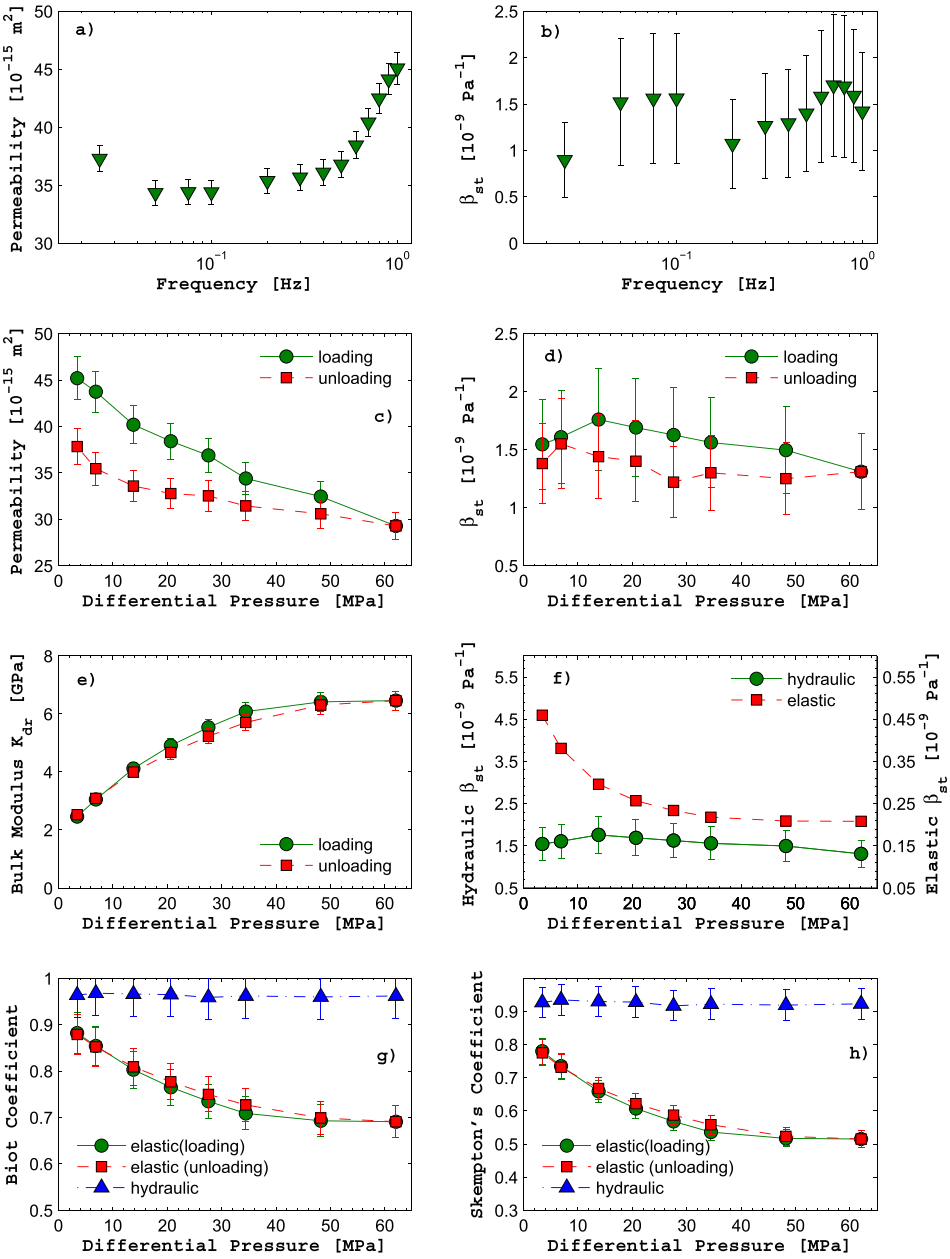

FIG. 10. Data measured on the Fox Hills 7 sample. [(a) and (b)] Measured permeabilities and storage capacities as a function of oscillation frequency. 1 mD approximately equals to 9.86 $\times$ 10^{-16} m^2. Note large error bars of the storage capacity values. (c) Measured values of permeability as a function of differential pressure at 0.1 Hz oscillation frequency, both loading and unloading pressure paths. (d) Values of storage capacity measured hydraulically as a function of differential pressure at 0.1 Hz oscillation frequency, both loading and unloading pressure paths. (e) The drained bulk modulus K_{dr} as a function of loading and unloading pressure paths. (f) Comparison between hydraulically and elastically derived storage capacities β_{st}, measured at 0.1 Hz oscillation frequency as a function of increasing differential pressure. Note the difference in y-axes scales. (g) Biot coefficient α as a function of loading and unloading differential pressures. Hydraulically derived Biot coefficients are marked by triangles and are highly overestimated. (h) Skempton's coefficient B as a function of loading and unloading differential pressures. Hydraulically derived Skempton's coefficients are marked by triangles and are highly overestimated.

more gradual and asymptotically reaches a background value that is dependent on stiff equant pores (Walsh, 1965). The "stiffening" of the rock with effective stress should lead to pressure-dependent Biot's and Skempton's coefficients, which gradually approach properties of a pure solid, i.e., the rock becomes insensitive to the pore pressure. Here we present the results of measurements of poroelastic properties as a function of applied effective hydrostatic stress. The drained bulk modulus K_{dr}, derived from direct K_{bp} measurements for the Fox Hills 7 sample at 0.1 Hz oscillation frequency, is plotted for both loading and unloading stresses in Fig. 10(e).

In this paper, we have demonstrated significant uncertainties in estimations of storage capacity from the hydraulic pore pressure oscillation method. However, since the storage capacity is an undrained poroelastic rock property, it can be inferred from the volumetric strain response to pore pressure oscillations. The main inputs for such calculations of storage capacity are K_{bp}, initial porosity ϕ, fluid K_{fl}, and mineral rock frame $K_{\min}$ bulk moduli [Eq. (9)]. Here, we assume that water compressibility as well as porosity does not change significantly with applied effective stress. A comparison of the elastically and hydraulically derived storage capacities are shown in Fig. 10(f). Note that the storage capacity is overestimated when derived only from the oscillating pore pressure method without independent strain measurements.

Furthermore, storage capacity estimates can be verified with Biot's and Skempton's coefficients. According to Eqs. (7)–(11), both α and B can be calculated from the storage capacity (β_{st}) and Biot's poroelastic expansion coefficient (K_{bp}). The two independent measurements of storage capacity yield independent estimates of Biot's and Skempton's coefficients [Figs. 10(g) and 10(h)]. Biot's and Skempton's

coefficients derived from hydraulically measured storage capacity are close to 1; such high values are more indicative of unconsolidated sediments or soils. In contrast, α and B derived from elastic strain measurements present a more realistic picture with pressure dependent Biot's and Skempton's coefficients.

V. CONCLUSIONS

Our oscillating pore pressure apparatus is capable of simultaneously measuring permeability, storage capacity, and drained poroelastic properties as functions of oscillation frequency and effective stress. The lower frequency limit presented here is 0.01 Hz although the apparatus can oscillate at much lower frequencies. The upper frequency limit (~1 Hz) is limited due to equipment constraints.

We performed a detailed sensitivity analysis according to the reported procedures (Bernabé *et al.*, 2006). The average error in storage capacities was established to be approximately 50%, peaking at 120% at lower oscillation frequencies. Despite the fact of ambiguous storage capacity measurements, the estimation of permeability was still quite precise with average errors not exceeding 10%.

We show that selection of the downstream reservoir requires judicious balance between the signal quality and error minimization. Thus, the high porosity and permeability of the rock sample necessitated using a large downstream reservoir for measurable amplitude ratios and phases. The large downstream reservoir, however, shifted the possible (R, θ) solutions toward the solution boundary and led to large errors in storage capacity estimates.

We present two sample data sets of transport and poroelastic properties measured at functions of oscillation frequency and effective stresses with our apparatus. The data sets are a benchmark test with a capillary tube and rock sample test with the Fox Hills sandstone. Although dynamic permeability should be independent of frequency, we do measure a sharp increase in permeability starting at 0.3 Hz. The measured transport and poroelastic properties follow the known pressure trends: permeability decreases and moduli increase with hydrostatic load, initially due to the closure of microcracks and compliant pores.

Comparisons of storage capacities from hydraulic measurements and from strain measurements as well as poroelastic coefficients (Biot and Skempton's coefficients) showed significant differences. An overestimation of storage capacity can be related to the large absolute errors in the hydraulically derived values. Furthermore, the measured rock sample appears to behave similar to soils, as deduced from the hydraulic measurements. Strain measurements yield more realistic values.

ACKNOWLEDGMENTS

This work was sponsored by Fluids/DHI (this is the name of one consortium) and OCLASSH consortia at Colorado School of Mines. Dr. Robert Kranz helped tremendously at initial stages of setup building; we also thank him for fruitful discussions. We are grateful to Dr. Jörg Renner and an anonymous reviewer for their helpful comments and suggestions. Dr. Mike Batzle has passed away by the time of this manuscript submission, a legendary rock physicist, our dear mentor, colleague, and friend; he will forever remain in our hearts.

APPENDIX: AN EXACT EXPRESSION FOR STORAGE CAPACITY OF A CAPILLARY TUBE

We begin with the equation of pore compressibility [K_{pc} in the work of Zimmerman *et al.* (1986)] for a single needle-like prolate cylindrical pore, as given by Mavko *et al.* (2009),

$$\frac{1}{K_{pc}} = -\frac{1}{V_p}\left(\frac{\partial V_p}{\partial P_c}\right)_{\delta P_p = 0} = \frac{5 - 4\nu_s}{3K_s(1 - 2\nu_s)}, \tag{A1}$$

where V_p is the pore volume, P_c is the confining pressure, P_p is the pore pressure, and K_s and ν_s are, respectively, the bulk modulus and Poisson's ratio of the material, hosting the cylindrical pore. We can relate pore compressibility K_{pc} to pseudo-bulk modulus K_{bp} by the following equation [e.g., Wang (2000) and Kümpel (1991)]:

$$\frac{1}{K_{bp}} = \frac{\phi}{K_{pc}}. \tag{A2}$$

Equation (9) in terms of K_{pc} becomes

$$\beta_{st} = \phi\left(\frac{1}{K_{pc}} - \frac{1}{K_{\min}} + \frac{1}{K_{fl}}\right). \tag{A3}$$

For the case of a fluid-filled capillary $\phi = 1$ and $K_{\min} = K_s$, we arrive at the final equation of storage capacity of a single needle-shaped pore by substituting Eq. (A1) into Eq. (A3),

$$\beta_{st} = \frac{2}{3K_s}\left(\frac{1 + \nu}{1 - 2\nu}\right) + \frac{1}{K_{fl}}. \tag{A4}$$

Batzle, M. L., Simmons, G., and Siegfried, R. W., "Microcrack closure in rocks under stress: Direct observation," J. Geophys. Res. **85**, 7072–7090, https://doi.org/10.1029/jb085ib12p07072 (1980).

Bennion, D. W. and Goss, M. J., "A sinusoidal pressure response method for determining the properties of a porous medium and its in-situ fluid," Soc. Petrol. Eng. **SPE 3541**, SPE-3541-MS (1971).

Bernabé, Y., Mok, U., and Evans, B., "A note on the oscillating flow method for measuring rock permeability," Int. J. Rock Mech. Min. Sci. **43**, 311–316 (2006).

Bernabé, Y., Mok, U., Evans, B., and Herrmann, F. J., "Permeability and storativity of binary mixtures of high- and low-permeability materials," J. Geophys. Res. **109**, B12207, https://doi.org/10.1029/2004jb003111 (2004).

Brace, W. F., Walsh, J. B., and Frangos, W. T., "Permeability of granite under high pressure," J. Geophys. Res. **73**, 2225–2236, https://doi.org/10.1029/jb073i006p02225 (1968).

Faulkner, D. R. and Rutter, E. H., "Comparisons of water and argon permeability in natural clay-bearing fault gouge under high pressure at 20 C," J. Geophys. Res. **105**, 16415–16426, https://doi.org/10.1029/2000jb900134 (2000).

Fischer, G. J., "The determination of permeability and storage capacity: Pore pressure oscillation method," in *Fault Mechanics and Transport Properties of Rocks*, edited by Evans, B. and Wong, T.-F. (Academic Press, 1992), pp. 187–211.

Geertsma, J., "Land subsidence above compacting oil and gas reservoirs," J. Pet. Technol. **25**, 734–744 (1973).

Green, D. H. and Wang, H. F., "Specific storage as a poroelastic coefficient," Water Resour. Res. **26**, 1631–1637, https://doi.org/10.1029/wr026i007p01631 (1990).

Guéguen, Y., Adelinet, M., Ougier-Simonin, A., Fortin, J., and Schubnel, A., "How cracks modify permeability and introduce velocity dispersion: Examples of glass and basalt," Leading Edge **30**, 1392–1398 (2011).

Guéguen, Y. and Palciauskas, V., *Introduction to the Physics of Rocks* (Princeton University Press, 1994).

Hofmann, R. and Batzle, M. L., "Grain modulus," Technical Report No. 1, Fluids/DHI Consotium Technical Reports, 2005.

Hsieh, P. A., Tracy, J. V., Neuzil, C. E., Bredehoeft, J. D., and Silliman, S. E., "A transient laboratory method for determining the hydraulic properties of 'tight' rocks—I. Theory," Int. J. Rock Mech. Min. Sci. Geomech. Abstr. **18**, 245–252 (1981).

Hughes, E. R., Leighton, T. G., Petley, G. W., White, P. R., and Chivers, R. C., "Estimation of critical and viscous frequencies for Biot theory in cancellous bone," Ultrasonics **41**, 365–368 (2003).

Johnson, D. L., Koplik, J., and Dashen, R., "Theory of dynamic permeability and tortuosity in fluid-saturated porous media," J. Fluid Mech. **176**, 379 (1987).

Kranz, R. L., Saltzman, J. S., and Blacic, J. D., "Hydraulic diffusivity measurements on laboratory rock samples using an oscillating pore pressure method," Int. J. Rock Mech. Min. Sci. Geomech. Abstr. **27**, 345–352 (1990).

Kümpel, H. J., "Poroelasticity: Parameters reviewed," Geophys. J. Int. **105**, 783–799 (1991).

Kurzeja, P., Steeb, H., Strutz, M. A., and Renner, J., "Oscillatory fluid flow in deformable tubes: Implications for pore-scale hydromechanics from comparing experimental observations with theoretical predictions," J. Acoust. Soc. Am. **140**, 4378–4395 (2016).

Makhnenko, R. M. and Labuz, J. F., "Unjacketed bulk compressibility of sandstone in laboratory experiments," in *Poromechanics V: Proceedings of the Fifth Biot Conference on Poromechanics* (ASCE, 2013), pp. 481–488.

Mavko, G., Mukerji, T., and Dvorkin, J., *The Rock Physics Handbook: Tools for Seismic Analysis of Porous Media* (Cambridge University Press, 2009).

Philip, R. B. and Robinson, D. K., *Data Reduction and Error Analysis for the Physical Sciences* (McGraw Hill, 2003).

Pride, S., "Relationships between seismic and hydrological properties," in *Hydrogeophysics* (Springer, 2005), pp. 253–290.

Rigord, P. and Caristan, Y., "Analysis of porous media heterogeneities using the diffusion of pressure waves," J. Geophys. Res. **98**, 9781–9791 (1993).

Sheng, P. and Zhou, M. Y., "Dynamic permeability in porous media," Phys. Rev. Lett. **61**, 1591–1594 (1988).

Song, I. and Renner, J., "Experimental investigation into the scale dependence of fluid transport in heterogeneous rocks," Pure Appl. Geophys. **163**, 2103–2123 (2006).

Song, I. and Renner, J., "Analysis of oscillatory fluid flow through rock samples," Geophys. J. Int. **170**, 195–204 (2007).

Tardif, E., Glover, P. W. J., and Ruel, J., "Frequency-dependent streaming potential of Ottawa sand," J. Geophys. Res. **116**, B04206, https://doi.org/10.1029/2010jb008053 (2011).

Wagner, H., Bedorf, D., Küchemann, S., Schwabe, M., Zhang, B., Arnold, W., and Samwer, K., "Local elastic properties of a metallic glass," Nat. Mater. **10**, 439–442 (2011).

Walsh, J. B., "The effect of cracks on the compressibility of rock," J. Geophys. Res. **70**, 381–389, https://doi.org/10.1029/jz070i002p00381 (1965).

Wang, H. F., *Theory of Linear Poroelasticity With Applications to Geomechanics and Hydrogeology* (Princeton University Press, 2000).

Zhou, M. Y. and Sheng, P., "First-principles calculations of dynamic permeability in porous media," Phys. Rev. B **39**, 12027–12039 (1989).

Zimmerman, R. W., Somerton, H. W., and King, M., "Compressibility of porous rocks," J. Geophys. Res. **91**, 765–777, https://doi.org/10.1029/jb091ib12p12765 (1986).